Thermodynamic and kinetic controls on co-transport of *Pantoea agglomerans* cells and Zn through clean and iron oxide coated sand columns.

Leon Kapetas[a,*], Bryne T. Ngwenya[a], Alan M. MacDonald[b] and Stephen C. Elphick[a].

[a] School of Geosciences, Earth Subsurface Research Group, Grant Institute, University of Edinburgh, West Mains Road, Edinburgh EH9 3JW, United Kingdom

[b] British Geological Survey, Murchison House, West Mains Road, Edinburgh EH9 3LA, United Kingdom

[*]Corresponding author. Tel: +44 (0) 1316508507, email: leonkapetas@gmail.com

Abstract

Recent observations that subsurface bacteria quickly adsorb metal contaminants raise concerns that they may enhance metal transport, given the high mobility of bacteria themselves. However, metal adsorption to bacteria is also reversible, suggesting that mobility within porous medium will depend on the interplay between adsorption-desorption kinetics and thermodynamic driving forces for adsorption. Till now there has been no systematic investigation of these important interactions. This study investigates the thermodynamic and kinetic controls of co-transport of *Pantoea agglomerans* cells and Zn in quartz and iron-oxide coated sand (IOCS) packed columns. Batch kinetic studies show that significant Zn sorption on IOCS takes place within two hours. Adsorption onto *P. agglomerans* surfaces reaches equilibrium within 30 minutes. Experiments in flow through quartz sand systems demonstrate that bacteria have negligible effect on zinc mobility, regardless of ionic strength and pH conditions. Zinc transport exhibits significant retardation in IOCS columns at high pH in the absence of cells. Yet, when mobile bacteria (non attached) are passed through simultaneously with zinc, no facilitated transport is observed. Adsorption onto cells becomes significant and plays a role in mobile metal speciation only once the IOCS is saturated with zinc. This suggests that IOCS exhibits stronger affinity for Zn than cell surfaces. However, when bacteria and Zn are pre-associated on entering the column, zinc transport is initially facilitated. Subsequently, zinc partly desorbs from the cells and redistributes onto the IOCS as a result of the higher thermodynamic affinity for IOCS.

1. Introduction

The presence of colloids, including bacteria, can affect metal contaminant mobility in natural aquifer systems. Provided that a contaminant adsorbs onto the colloid, the presence of colloids can lead to facilitation and/or attenuation of the contaminant's transport [1, 2]; in media with some degree of physical heterogeneity, colloid facilitated transport can take place through macropores and concurrent colloid-assisted contaminant retention can be observed in small pores. In addition, it has been shown that minor differences in physical properties of cells can lead to major differences in their transport behaviour in the field environment [3]. Such differences are expected to be reflected in the mobility of the contaminant adsorbed on the cells. Microbial cell surfaces show strong affinity for a variety of metals [4-8]. These observations have significant potential environmental implications, and demand that enhanced mobilisation scenarios be taken into consideration in assessing risk from contamination sources [9]. Pang et al. [10] showed that Cd travelled through a gravel column 17-20 times faster in the presence of bacteria, although during the desorption phase bacteria slowed down Cd breakthrough by 2-3 times. Chen et al. [11] found that Cs transport through a sediment column was facilitated when it was pre-associated with colloids, however at low flow rates Cs would be stripped off the colloid, therefore revealing that desorption was a residence-time-dependent process and facilitation depends on process kinetics. In another study, the facilitated transport of Pb was suppressed by the injection of high concentration of divalent salts, such as Ca^{2+}, as colloid release from the solid matrix was reduced [12]. In a field study by Pang and Close [13], multiple simultaneous peaks of bacteria and Cd breakthrough curves (BTCs) were observed, revealing the strong effect of bacteria-facilitated transport. An early Cd peak coincided with a *B. subtilis* peak and occurred before the conservative tracer arrival, suggesting the high degree of association of Cd with bacteria which followed preferential flow paths. Moreover, Bekhit et al. [14] demonstrated that the degree of colloid facilitation depends on the chemical conditions of the system; colloid mediated transport of Sr depended primarily on ionic strength (*I)* and secondarily on pH. Other studies have shown that the presence of colloids increased the transport velocity of Cu and Zn by 5 to 50 times and that of Pb by 10 to 3000 times [15, 16]. Additionally, Roy and Dzombak [17] showed that Ni^{2+} cations exhibited faster breakthrough in sand columns when in situ colloids were mobilised. Lastly, Sen et al. [18] demonstrated that kaolin colloids can lead to

increased retardation of Ni^{2+} cations depending on the porous medium grain to colloid size ratio.

The apparent dependence of facilitated transport on solution chemistry and flow rate points to complex interplay between thermodynamic and kinetic controls on colloid-metal co-transport. Bacteria are ubiquitous in subsurface environments but to date there has been no systematic experimental study examining the relative significance of thermodynamic and kinetic controls on the mobility of metals in mixed metal-bacteria systems. Here, we examine this problem by conducting metal-bacteria co-transport experiments using two injection scenarios: (i) co-injection experiments in which cells and Zn are mixed at the column inlet to examine the relative partitioning of metal between bacteria, fluid and the porous medium, and (ii) injection of cells pre-adsorbed with Zn to examine whether Zn will re-distribute between phases.

2. Materials and methods

2.1. Cell culture and preparation

The Gram-negative bacterium *Pantoea agglomerans* (also known as *Enterobacter agglomerans* [19]) was used for the purpose of this study because (a) its surface chemistry has been well characterized [20] and (b) it forms mono-dispersed suspensions allowing reproducible cell transport behaviour. Fresh cell batches were cultured after the method of Tourney et al. [21] in two successive stages. First, 250 mL Pyrex flasks containing 100 mL sterilised Lysogeny Broth growth medium (30 g L^{-1} tryptone, 5 g L^{-1} yeast extract) were inoculated from primary cultures kept in agar plates. Growth medium in the Pyrex flasks was sterilised before use by autoclaving at 121^{o}C for 30 minutes. The 100 mL cultures were then incubated for 16 hours at 30^{o}C and were harvested in their stationary growth phase. In the second stage, 2 L Pyrex flasks containing 1 L of the same growth medium were inoculated with 5 mL of the 100 mL cell suspension. The 1 L cultures were subsequently incubated under the same conditions. This procedure was followed in order to achieve a final homogeneous cell suspension for use in the experiments. Cells were then harvested by centrifugation (Sorvall RC6 centrifuge) at 19,300 g for 15 minutes at 4 ^{o}C and washed three times with 18 MΩ ultrapure water (Purite Ltd). Cell dimensions were determined on scanning electron microscope images of *P. agglomerans* cells [8], at 1.1 ± 0.3 μm and 0.49 ± 0.04 μm (mean± st. deviation) for length and width respectively. The isoelectric

point of *P. agglomerans* cells has been measured and is approximately 2.1 (Figure S.4 of the Supporting Infrmation (SI) document).

2.2. Mineral preparation

General purpose silica sand (Fisher Scientific) was first sieved with stainless steel sieves to a grain size range 120-350 μm. Grain size distribution was determined on a sample of 2 g using a Beckman Coulter LS Particle Size Analyser. Characteristic size distribution values are d_{50} = 212 μm and uniformity coefficient d_{60}/d_{10} = 1.40. After heating at 550^{o}C for 48 hours to destroy organic materials [22], sand was rinsed with ultrapure (18 MΩ) water. In order to remove metal traces sand was soaked in 2.87 M HNO_3 for 24 hours [23]. The acid solution was then decanted and the sand was rinsed repeatedly with ultrapure water until the pH of the supernatant was approximately equal to the pH of the point of zero charge (pH_{zpc}) of the silica sand [23]. Further, the sand was agitated in a suspension with pH close to 10 for 2 hours in order to remove readily soluble silica and remaining colloids [22]. The sand was again rinsed several times with ultrapure (18 MΩ) water and washed in 0.001 M HNO_3 for 12-14 hours to remove any remaining cations [24]. Finally, the sand was washed several times with ultrapure water to pH close to the pH_{zpc}. The final sand product was used in the "clean sand" experiments.

An Fe coating was added to a portion of the clean sand to obtain the Iron Oxide Coated Sand (IOCS). The iron oxide coating increases the surface area of the sand and increases metal affinity compared to the uncoated silica [25]. The coating did not alter the particle size distribution compared to the uncoated material. The preparation procedure was adapted from Schwertmann [26] and Yee and Fein [23]. First, batches of polyethylene bottles containing 100 g of clean sand were mixed with 10.36 g $Fe(NO_3)_3$ in 1 L of ultrapure (18MΩ) water. The content was continuously stirred while aliquots of 6 M NaOH were added until the suspension pH reached 6. The bottles were shaken on a rotor overnight to enhance contact of the sand grains with the solution. Samples were then washed in a 1 M $NaNO_3$ solution with pH close to three. This procedure allowed the coated sand with strongly bound iron oxide particles to be separated from weakly attached iron oxide aggregates [26]. The coated grains were then rinsed repeatedly until all free Fe and Fe precipitates were removed from the solution. Finally, the coated grains were oven-dried at 60^{o}C [27]. XRF

analysis (Philips 2404 spectrometer) showed that clean sand contains 99.3% silica, while the Fe content of IOCS was measured at 17.90 mol Kg^{-1}. Result for Fe content was confirmed with Aqua-regia digestion to within 1% difference.

2.3. Zinc adsorption experiments

Cells were washed three additional times in $NaClO_4$ electrolyte, whose ions exhibit minimal binding onto the mineral and bacterial surfaces, of the same concentration used in the Zn batch adsorption experiments. Selected cell concentrations for the adsorption experiments were 0.25 and 0.5 g L^{-1} dry biomass, and zinc concentration was 1.53×10^{-4} M. We selected low biomass: metal ratios to resolve adsorption among functional group sites at higher pH 6.5-7.5 conditions [28], and also to match concentrations used in flow experiments as more concentrated suspensions could clog up the columns. A mass concentration of 0.5. g L^{-1} dry biomass is equivalent to a cell density of approximately 5×10^{8} cells mL^{-1}, lying between 10^{7} cells mL^{-1} which is typical for pristine groundwater and 10^{9} cells mL^{-1} which is typical for soil environments [29, 30].

The following solution preparation procedure was followed to avoid the "acid shock" of the cells [31]. A 400 mL 1.91×10^{-4} M Zn solution was prepared (from a standard solution 1.53×10^{-2} M $Zn(NO_3)_2.4H_20$ in 0.5 M HNO_3, Fisher Scientific) and its pH was increased to approximately 4. Then, a 100 mL (1.25 or 2.5 g L^{-1} dry biomass) cell suspension was prepared and the pH was adjusted to approximately 4 by adding a known volume of 0.1 M HNO_3. Lastly, the cell suspension was mixed with the zinc solution to obtain the final cell-zinc suspension concentrations (0.25 or 0.5 g L^{-1} dry biomass – 1.53×10^{-4} MZn). Five mL sub-samples were collected in glass vials in triplicate to calculate the dry mass of suspensions. Sub-samples were evaporated to dryness at 50^{o}C until no change in weight was observed. Dry weights were corrected for electrolyte contribution.

Cell-zinc adsorption experiments were carried out at a pH above 3.5 to avoid cell lysis [31] and below 7.5 to avoid Zn precipitation based on Visual MINTEQ calculations [32]. Sub-samples of 20 mL were taken from the suspension beaker in 30 mL reaction vessels that had been acid washed before. The pH was adjusted in the suspension beaker between successive sub-samples by adding a known amount of NaOH to

obtain samples in the desired pH range. After equilibration for 30 minutes 10 mL were then drawn with a 10 mL syringe and filtered with 0.20 μm filters into 30 mL acid washed plastic bottles. Bottle samples were subsequently acidified (11 M HNO_3, Fisher Scientific) and kept at 4°C. They were analysed for dissolved Zn concentration with an Varian Spectra AA300 atomic absorption spectrophotometer using an air/acetylene flame at a wavelength of 213 nm. RSD analytical precision was between 0.1 and 2.2% for all samples measured. The final pH of the remaining suspension was measured immediately in the tubes. Samples of Zn solution equilibrated in tube reactors without bacteria were taken for control. Control samples were taken to measure the initial concentration of Zn in suspension. Zinc adsorption onto the tubes was not detected.

Kinetics of Zn adsorption onto *P. agglomerans* were also investigated at pH 7 by rotating reaction vessels on a rotating rack for varying time periods. Kinetics of zinc adsorption onto IOCS were investigated at pH 7 in reaction vessels containing 7.5 g IOCS and 1.53×10^{-4} M Zn in 27.5 mL suspensions. Moreover, a batch adsorption experiment at varying pH conditions was carried out for the IOCS adsorbent using the same concentrations as in the kinetic study.

Finally, surface complexation (SC) modelling of zinc adsorption onto both adsorbent surfaces was carried out using the optimization program FITEQL 4.0 [33]. Site concentrations used during adsorption modelling have been determined previously by modelling data of potentiometric titrations of *P. agglomerans* suspensions [20]. Several non electrostatic models were fitted to the adsorption data to test varying number/combinations of functional group types contributing to adsorption. The SC models are described in detail in the SI document. Briefly, as pH increases sites tend to deprotonate and subsequently adsorb Zn according to the following metal adsorption reaction:

$$R-A_i^- + Zn^{2+} \leftrightarrow R-A_iZn^+ \qquad (1)$$

where *R* denotes the bacterium where the functional group type, *A*, is attached. *R-A*$^-$ and *R-AH* represent deprotonated and protonated sites of the functional group respectively. A 1:1 stoichiometry was used to describe the Zn-functional group site adsorption complex [34], as other reaction stoichiometries were not supported due to

the poor fits of the models on the experimental datasets. Adsorption constants $K_{(i)ads}$ (i= 1, 2, 3…) are described using the following expression:

$$K_{(i)ads} = \frac{[R - A_i Zn^+]}{[R - A_i^-][Zn^{2+}]} \quad (2)$$

where brackets represent the concentrations of the sites at equilibrium and [H^+] the activity of protons in solution.

2.4. Column experiments

2.4.1. Column preparation: Chromatography Omnifit borosilicate glass columns (25 mm internal diameter, 120 mm effective length, Sigma Aldrich) were wet packed with either clean or IOC sand. The water level was always kept 1-2 cm above the top of the sand surface. After each incremental addition of sand, the added sand was gently mixed with the lower surface layer of sand and then vibrated to minimize any settling and layering and to liberate any entrapped air [35]. Sand was always poured in small quantities from a low height and care was taken to avoid heap formation which often leads to particle size segregation [36]. Average porosity of packed columns was 0.40. The packed column was sealed with PTFE end fittings containing 40 μm polyethylene (PE) porous frits which support the sand and dispense the fluid and the bacteria. The base of the vertical column was connected through 1/16" PTFE tubing to a Masterflex peristaltic pump (Cole Palmer Instruments). A three way T-piece/valve connected the two influent containers with the pump. The effluent was collected at the column top outlet for AAS analysis and bacterial optical density measurement (CamSpec M501, wavelength 600 nm). Perfect mixing of solutions was tested; a dye tracer-zinc solution and a bacterial suspension were passed through the T-piece. The tracer, diluted by 50%, distributed homogeneously across the sand column.

2.4.2. Column conditioning: Sand columns were equilibrated with 10 pore volumes (PV) of ultrapure water. Subsequently 10 PV of the buffer/background electrolyte solution were pumped through to stabilise column pH and ionic strength to the suitable experimental conditions. 2-(N-morpholino) ethanesulfonic acid (MES) and 3-(N-morpholino) propanesulfonic acid (MOPS) buffers were used to achieve pH 5.3 or 7 respectively. The cell/Zn solution with the same buffer and electrolyte concentration was then pumped through at 2 mL min^{-1} until complete breakthrough.

2.4.3. Effluent sampling: 14 mL of effluent collected in 15 mL test tubes were prepared for analysis immediately after collection. Seven mL were immediately filtered through 0.20 μm filters to prevent potential post-sampling desorption of Zn from the cell surfaces and acidified to measure free aqueous zinc concentration. Cell concentration was measured with a UV-VIS spectrophotometer (CamSpec M501) at wavelength λ= 600 nm in the remaining 7 mL, which were subsequently acidified, equilibrated to allow zinc desorption, and then filtered to measure the total mobile zinc concentration.

2.4.4. Column experimental procedures: Two different column experimental procedures were followed in this study, all run in duplicates:

1. A cell suspension containing 1 g L^{-1} dry mass cell concentration was mixed with a 3.06×10^{-4} M Zn solution just before entering the packed column. Mixing took place at the T-piece before the inlet to the column. The dead volumes of the system were minimised so that the contact time between the cells and zinc did not exceed 3 seconds before reaching the inlet. In entering the column, zinc was "free" to distribute among the solid, cell and aqueous phase. The mixing resulted in a 50% dilution of both solutions, i.e. the final input concentrations were 1.53×10^{-4} M Zn and 0.5 g L^{-1} dry mass which are the same as the concentrations used in the batch adsorption experiments. For a flow rate of 2 mL min^{-1}, the residence time for 1 PV was approximately 14 minutes. Cell suspensions supplying the sand columns were replenished approximately every 60 minutes to avoid cell death or DOC production [20].

2. For the second experimental procedure, 1.53×10^{-2} M Zn were pre-equilibrated with 0.5 g L^{-1} dry mass concentration of a cell suspension before entering the column. Equilibration took place for approximately 30 minutes before entering the column.

In addition, zinc flow column experiments were run in the absence of bacteria to serve as control. These experiments were run under the same mineralogical and chemical conditions as the co-transport experiments. In addition, breakthrough curves of 9.2×10^{-5} M and 1.53×10^{-4} M Zn influent through an IOCS column were compared.

They both exhibited the same characteristic breakthrough time which suggests that Zn adsorption onto IOCS follows a linear isotherm for the experimental concentration range.

2.4.5. Breakthrough curve modelling

The Stanmod-CFITIM equilibrium model [37] was used to model zinc breakthrough curves. The selected equilibrium model ignores chemical non-equilibrium effects which act during the experiments as will be discussed; it is used merely to obtain the value of the retardation factor (RF) to allow comparisons among different experiments. The model focuses on fitting the zinc BTC at the location where C/C_o = 0.5 and provides an uncertainty estimation of the retardation factor, namely the standard error of regression coefficient, based on the goodness of fit. Model fits are not presented, rather interest is focused on the obtained retardation factors which are summarised in Table 1.

3. Results

3.1. Batch adsorption experiments

Experimental results showing the kinetics of zinc adsorption onto both adsorbent surfaces are provided in Figure S.1 of the SI document. Zinc adsorption onto *P. agglomerans* surfaces reaches 90% of its maximum value after approximately 30 min during an initially rapid adsorption phase, which is consistent with previous studies [34, 38]. Maximum adsorption is reached after approximately 100 minutes. Rapid adsorption onto IOCS takes place within 2 hours at pH 7. Slow adsorption continues to take place for longer likely due to micropore diffusion [39]. Adsorption onto IOCS at sub neutral pH 5.3 conditions was negligible, while adsorption onto clean sand was minimal throughout the pH range (results not shown).

Adsorption kinetics also showed that 80% of zinc adsorption onto cells takes place within the first 10 minutes of contact time. For zinc adsorption onto IOCS, 70% takes place within the first 10 minutes of contact time. This suggests that allowing a 10-15 minute influent residence time during column experiments is sufficient for bulk adsorption to be completed; nevertheless, variations in adsorption speed are expected within a column environment as the contact conditions are modified compared to a batch reactor.

Figure S.2 shows that pH influences zinc adsorption onto *P. agglomerans* surfaces dramatically. When pH increases, more functional group sites of the cell wall surface deprotonate attaining a negative charge, which allows further metal adsorption to take place [4, 28, 40]. Moreover, adsorption increases as biomass concentration increases. Biomass normalised zinc adsorption is comparable to that of another Gram negative *E. coli* [41], suggesting that *P. agglomerans* exhibits typical adsorption behaviour. Moreover, the batch experiment of zinc adsorption onto IOCS (Figure S.3) demonstrates strong dependence on pH.

Table S.2 provides the surface complexation adsorption constants and site concentrations of the two zinc adsorbing cell surface sites for both *P. agglomerans* and IOCS surfaces. A two site non-electrostatic adsorption model best described the adsorption data (Table S.1). Similarly, a two site non-electrostatic model was chosen to describe zinc adsorption onto IOCS. Experimental data and modelled curves are provided in section S.2 of the SI. A comparison of the acidity constants (Table S.2) shows that bacterial surface sites deprotonate at a lower pH than IOCS sites and thus can take up metals at more acidic conditions. However, a comparison of the adsorption constants indicates that, at higher pH, zinc adsorption is more favourable on IOCS sites as they deprotonate.

3.2. Co-transport of Zn and cells without prior association

In clean sand columns, zinc and *P. agglomerans* cells were co-transported without pre-association. Figure 1A shows that, at pH 7 and *I* 0.01 M, concentrations of total zinc breaking through in the absence or presence of cells are similar and, hence, cells have little effect on total zinc mobility (in all figures, bromide was used as the conservative tracer for column flow characterization and error bars have been omitted for clarity; average 2σ values are ±0.06 and ±0.08 for zinc and cell concentrations respectively). The calculated retardation factors for the experiments in the absence (Zn- no cells) and presence of cells (total Zn) are presented in Table 1. The retardation factor of free Zn was calculated after normalising the BTC data by dividing each C/C_o observation by the steady state concentration ($C/C_o = 0.74$). Zinc partitions between the fluid (60%), cells (30%) and clean sand (10%), in the period between 2-9 PVs. After 9 PVs, steady state is reached, whereby cell-bound mobile zinc accounts for

approximately 25-30% of the total zinc that breaks through (Table 1). These results were anticipated as cells and zinc both exhibit a slight retardation (RF<2) relative to the bromide conservative tracer when they travel through clean sand columns.

Figure 1B presents BTCs from a co-transport experiment in an IOCS column carried out at pH 5.3 and *I* 0.01 M. At this particular pH only a negligible fraction of the influent zinc is expected to adsorb onto the IOCS (see Figure S.3). Hence, in the absence of cells zinc exhibits a slight retardation (RF=1.42). During co-transport, cells breakthrough ($C/C_o = 0.5$) approximately 3 PVs later than zinc. This is due to the negative surface charge of cells at pH 5.3, as measured experimentally (see Figure S.4. in SI), which results in their strong electrostatic attachment on the positively charged IOCS [42]. Cell straining is not thought to contribute significantly to the observed cell removal. The degree of straining is governed by the shorter of the two cell dimensions (0.49 μm), as cells tend to align themselves to the flow direction [43]. The ratio of cell to grain particle diameter in these column experiments is approximately 0.0023, significantly lower than 0.05 which has been the reported threshold value at which straining becomes significant [44]. However, ratios as low as 0.0017 have been associated with straining [35, 45, 46]. Moreover, the ratio of cell to average grain size in silica sand and IOCS packed columns is maintained the same, and hence differential straining behaviour is not anticipated. On the other hand, the gradual approach to peak breakthrough concentrations which is a common feature to silica and IOC sand packed columns could be attributed to straining [35]. Further experimental work and modelling would be required to attest this.

Despite absolute cell retention in this initial period, zinc breaks through with only little retardation compared to zinc in the absence of cells or to a conservative tracer (RF=1.54). Concentrations of total zinc are similar to concentrations of free zinc for PV< 4, indicating zinc transport was not associated with bacteria despite the fact that some zinc is expected to associate with *P. agglomerans* cells at these pH conditions (Figure S.2). This suggests that the different relative velocities of cells and zinc in the column lead to their chromatographic separation which reduces their contact time leading to adsorption. As more cells breakthrough at later PVs, free aqueous zinc decreases due to the increase in cell-bound mobile zinc (Fig. 1B).

Figure 1C presents experimental BTCs obtained at pH 7. Zinc in the control experiment (no cells) breaks through with significant retardation after 8 PVs. Thereafter, zinc adsorption becomes rate limited and takes place at a slower rate. Hence, zinc does not reach 100% breakthrough even after 25 PVs, which is consistent with the observations from the batch kinetic experiments showing that slow sorption continues to take place even after 420 minutes (see Figure S.1). An apparent zinc dispersion effect takes place due to this slow adsorption kinetics mechanism. It is noted that during co-transport total Zn breaks through with only a limited delay compared to the control experiment. This is also reflected in the values of the retardation factor (Table 1), which equals 8.88±0.31 and 10.15±0.68 for the control and the co-transport experiment respectively. Thus, cells do not act strongly as a conveyor belt for zinc as would be expected, despite the fact that (i) cells have strong affinity for zinc at pH 7 and (ii) they travel much faster than zinc. Chromatographic separation is less likely to take place as both cells and zinc are initially retarded and thus sufficient contact time is allowed. It becomes apparent that the IOCS and cell surface adsorbents compete for the available free zinc of the influent solution. These results imply the thermodynamic control over the adsorption, such that cells do not play a significant role on zinc transport or immobilisation. This is clearly reflected in the calculated adsorption constants (K_{ads}) for Zn to the two surfaces, which are higher for IOCS by at least 3 orders of magnitude (see Table S.2). Once kinetics of adsorption onto IOCS is slow enough, zinc is found in solution and uptake by cells can take place. This is noted in the effluent after 9 PVs: cells affect the distribution of zinc between cell-bound mobile and free species, only when bulk fast adsorption onto the IOCS has been completed. At apparent steady state conditions (after 16 PVs), the equilibrium concentrations of zinc adsorbed onto *P. agglomerans* surfaces are in agreement with the batch adsorption experimental results (Fig. S.1). It is noted that non linearity of adsorption would lead to non-overlaying BTCs. This would invalidate the comparison of arrival time and peak concentration between the BTCs of zinc-no cells and total zinc (calculated as the sum of free-zinc BTC and mobile cell-bound zinc BTC). As mentioned in section 2.4.4, zinc adsorption is linear in the experimental concentration range used.

3.4. Co-transport of Zn associated with cells

An additional column co-transport experiment was carried out following the second experimental procedure of section 2.4. Cells and zinc were pre-associated at pH 7, *I* 0.01 M before entering the IOCS column which resulted in approximately 40% of Zn being cell-bound. Under this experimental scenario (Fig. 2), cell mobility was initially attenuated similarly to Figure 1C. Zeta potential measurements (SI, section S.3, Figure S.4) showed that adsorption of zinc to cells did not significantly reduce the negative zeta potential and thus did not decrease the electrostatic adsorption to IOCS. It is observed (Fig. 2) that after the first 3 PVs, 20% of cells breakthrough in the effluent. Yet, cell-bound mobile zinc is not measured in the effluent suggesting that zinc was stripped off the surface of *P. agglomerans* cells and adsorbed onto the IOCS. However, in the period between the 3rd until 6th PV mobile zinc appears in the effluent. Free zinc concentration is practically zero while total zinc can be attributed to adsorbed mobile zinc (samples were filtered immediately after collection to avoid new equilibrium being attained in the collection tube; hence minimal zinc could desorb from the cell surfaces). This gives evidence of facilitated transport when cells and zinc are pre-associated on entering the column. Transport facilitation is reflected on the shape of the BTC of total zinc, and also in the lower value of the retardation factor (RF=7.60±0.25 for total Zn) in comparison to the control experiment (RF=8.88±0.31) shown in Table 1. Mobile cell-bound zinc breaks through 4 PVs earlier than previously, when cells and zinc were not pre-associated (Figure 1C), i.e. almost twice as fast.

Eventually, the amount of cell-bound zinc observed at apparent "steady state" (data after ~16 PVs) approximates the influent equilibrium concentration. At steady state approximately 0.45 g L^{-1} of cells (calculated as 0.9×0.5 g L^{-1}) adsorb 5.4×10^{-5} M Zn (calculated as (0.9-0.55) × 1.53×10^{-4} M). On the other hand, at the time corresponding to approximately 6PVs, 0.35 g L^{-1} of cells (calculated as 0.7×0.5 g L^{-1}) adsorb 2.3×10^{-5} M Zn (calculated as (0.15-0.00) × 1.53×10^{-4} M Zn). Therefore, the fraction of adsorbed mobile zinc is significantly less initially (e.g. at ~6 PVs, $2.3\times10^{-5}/0.35 = 6.57\times10^{-5}$ mol g^{-1}) than at equilibrium (either in the influent or at steady state where the adsorption fraction is $5.4\times10^{-5}/0.45 = 1.2\times10^{-4}$ mol g^{-1}). This observation suggests that zinc transfer from the cell surfaces to the IOCS continued also after the first 3 PVs flowed, suggesting reversibility of system reactions [6]. However, the residence

time was not sufficient for a new equilibrium to be attained, i.e. there was insufficient time for complete mass transfer of zinc from the cells to the IOCS.

4. Discussion

4.1. Mineralogical and chemistry controls

Mineralogy displayed a dominant effect on bacterial mobility. Cells broke through clean sand porous medium columns as fast as the conservative tracer. Cells were as mobile as zinc in the clean sand experiments and hence they only affected the distribution of mobile zinc. Significant cell retardation was observed when the medium was covered with an Fe coating. Yet, as was shown in Figure 1B, cells had negligible effect on zinc mobility in the IOCS column at below neutral pH conditions. Moreover, cells did not lead to enhanced mobility at pH 7 (Fig. 1C) despite the fact that they were significantly more mobile than zinc; this was due to the fact that their affinity for zinc was lower than that of IOCS.

However, it is possible that for different metal/colloid systems a specific pH range exists within which deprotonation of the colloid surface sites and metal adsorption onto them is thermodynamically supported, i.e. despite the greater adsorption contant $LogK_{ads}$ of the porous medium site-metal complex, the deprotonation constant $LogK_{\alpha}$ can be higher for colloid sites and hence adsorption will take place on the deprotonated colloid surface sites at a specific subneutral pH. Relative site concentrations for the porous medium and the colloid will also play a key role on relative metal adsorption. In the scenario where adsoption onto colloid surfaces dominates, colloid mobility will largely control metal transport.

4.2. Thermodynamic implications

It was shown that equilibrium assumptions are not met during column experiments when pre-association of cells and zinc takes place. This suggests that equilibrium assumptions are closely linked to the speed of the adsorption and desorption kinetics and the residence time; carrying out co-transport experiments at slower flow rates could highlight this effect. However, this was not done in the present study for fear of cell death and DOC production, either of which can influence adsorption. The flow rate in these experiments is typical of permeable aquifers while other aquifer systems can have slower velocities. Our results are not consistent with the finding of Turner

and Fein [47], who found that equilibrium assumptions are appropriate for the modelling of metal transport on bacteria bearing systems. In their study which used pre-associated suspensions of *B. subtilis* and Cd, Darcian velocity was 2.7 cm min^{-1}, which is an order of magnitude greater than ours, 0.41 cm min^{-1}. Hence, based on our findings their system was likely even further from equilibrium assumptions; however, it should be noted that their study made use of different adsorbent surfaces and sorbing metal. Despite the smaller value of Darcian velocity used in our study, non-equilibrium effects became evident. Thus, it is recommended that equilibrium conditions should not be assumed; instead they should be tested independently in each study. Kinetics should be carefully taken into consideration during experimental design (e.g. whether pre-association is allowed) and modelling work on the co-transport of colloids and metals. Steady state conditions were approximated only for the first type of experiments presented.

4.3. Environmental Relevance

The experimental application with the separate injection of the aqueous metal and the bacteria bears similarities to situations of contaminant metal spillage in soils containing colloids (e.g. bacteria) which can become mobilised [48, 49]. Also, this experimental design can be adopted to test the effectiveness of Permeable Reactive Barriers (PRBs) and filtration columns used for water decontamination [50, 51]; on the basis of our findings, IOCS PRBs or filters with similar characteristics are not expected to fail due to colloidal or bacterial plumes provided metal adsorption onto the filter is favourable and filter capacity is sufficient. In addition, the application of sewage sludge to farm land is an example of concurrent release of metal and bacterial loading which are commonly found in the sludge [52-55]; Metal exchange kinetics between competing adsorbent surfaces, such as those presented in this study, could potentially influence metal mobility.

A good understanding of metal adsorption/desorption kinetics and thermodynamic competition between different adsorbents is required to predict the fate of the metal in the natural system. It is currently a challenge to consider surface complexation within reactive transport modelling; such models could describe interactions between competing surfaces/metals and account for varying chemical conditions in an area that empirical sorption models have failed. However, they would require extensive input

data, including well constrained stability constants, well characterized mineralogy and knowledge of bacterial abundance.

The approach adopted in this study can be cautiously extrapolated to systems containing other bacterial species or metals with known stability constants, as it has been demonstrated that bacteria exhibit a universal (non specific to Gram grouping) proton and metal adsorption behaviour [56-58]. However, changes in cell growth phase will influence the values of the surface complexation constants [59, 60], and DOC commonly present in significant amounts in natural systems can modify our findings; DOC can potentially reduce adsorption of metals onto bacterial surfaces by acting as a competing complexing ligand [61, 62], facilitate contaminant transport [63] and also reduce cell deposition [64, 65]. Finally, the effect of extracellular polymeric substances (EPS) commonly produced by bacteria on metal mobility is still unclear; previous research has shown that EPS can either contribute to metal binding [66] or act as a protective barrier for metal adsorption onto cell walls, but also enhance bio-clogging and cell deposition that can indirectly hinder metal mobility [67-69].

Acknowledgements

We thank the Greek Scholarship Foundation and the School of Geosciences for funding this work. We also thank Ann Mennim for AAS analysis and Brian Berkowitz for recommendation on column experimental design. Constructive evaluation by three anonymous reviewers was very helpful in getting our message across.

Supporting Information Available

As noted in the text, this information is available free of charge via the Internet at http://pubs.acs.org/

References

1. McCarthy, J. F.; Zachara, J. M., Subsurface transport of contaminants. *Environ. Sci. Technol.* **1989,** *23*, 496-502.
2. Ryan, J. N.; Elimelech, M., Colloid mobilization and transport in groundwater. *Colloids Surf., A: Physicochemical and Engineering Aspects* **1996,** *107*, 1-56.
3. Becker, M. W.; Metge, D. W.; Collins, S. A.; Shapiro, A. M.; Harvey, R. W., Bacterial transport experiments in fractured crystalline bedrock. *Ground Water.* **2003,** *41*, (5), 682-9.
4. Burnett, P.-G. G.; Handley, K.; Peak, D.; Daughney, C. J., Divalent metal adsorption by the thermophile Anoxybacillus flavithermus in single and multi-metal systems. *Chem. Geol.* **2007,** *244*, (3-4), 493-506.
5. Deo, R. P.; Songkasiri, W.; Rittmann, B. E.; Reed, D. T., Surface complexation of Neptunium(V) onto whole cells and cell components of Shewanella alga: Modeling and experimental study. *Environ. Sci. Technol.* **2010,** *44*, (13), 4930-4935.
6. Fowle, D. A.; Fein, J. B., Experimental measurements of the reversibility of metal-bacteria adsorption reactions. *Chem. Geol.* **2000,** *168*, (1-2), 27-36.
7. Gorman-Lewis, D.; Fein, J. B.; Soderholm, L.; Jensen, M. P.; Chiang, M. H., Experimental study of neptunyl adsorption onto Bacillus subtilis. *Geochim. Cosmochim. Acta* **2005,** *69*, (20), 4837-4844.
8. Ngwenya, B. T., Enhanced adsorption of zinc is associated with aging and lysis of bacterial cells in batch incubations. *Chemosphere* **2007,** *67*, (10), 1982-1992.
9. Penrose, W. R.; Polzer, W. L.; Essington, E. H.; Nelson, D. M.; Orlandini, K. A., Mobility of plutonium and americium through a shallow aquifer in a semiarid region. *Environ. Sci. Technol.* **1990,** *24*, (2), 228-234.
10. Pang, L.; Close, M. E.; Noonan, M. J.; Flintoft, M. J.; van den Brink, P., A Laboratory study of bacteria-facilitated cadmium transport in alluvial gravel aquifer media. *J. Environ. Qual.* **2005,** *34*, (1), 237-247.
11. Chen, G.; Flury, M.; Harsh, J. B.; Lichtner, P. C., Colloid-facilitated transport of Cesium in variably saturated Hanford sediments. *Environ. Sci. Technol.* **2005,** *39*, (10), 3435-3442.
12. Grolimund, D.; Borkovec, M., Colloid-facilitated transport of strongly sorbing contaminants in natural porous media: Mathematical modeling and laboratory column experiments *Environ. Sci. Technol.* **2005,** *39*, (17), 6378-6386.
13. Pang, L.; Close, M. E., A field study of nonequilibrium and facilitated transport of Cd in an alluvial gravel aquifer. *Ground Water* **1999,** *37*, 785-792.
14. Bekhit, H. M.; Hassan, A. E.; Harris-Burr, R.; Papelis, C., Experimental and numerical investigations of effects of silica colloids on transport of strontium in saturated sand columns. *Environ. Sci. Technol.* **2006,** *40*, (17), 5402-5408.
15. Karathanasis, A. D., Subsurface migration of copper and zinc mediated by soil colloids. *Soil Sci Soc Am J: Madison, WI, ETATS-UNIS*, 1999; Vol. 63.
16. Karathanasis, A. D., Colloid-mediated transport of Pb through soil porous media*, International Journal of Environmental Studies, Volume 57, Issue 5*. Taylor & Francis: Colchester, 2000.
17. Roy, S. B.; Dzombak, D. A., Chemical Factors Influencing Colloid-Facilitated Transport of Contaminants in Porous Media. *Environ. Sci. Technol.* **1997,** *31*, (3), 656-664.
18. Sen, T. K.; Mahajan, S. P.; Khilar, K. C., Colloid-Associated contaminant transport in porous media: 1. Experimental studies. *AIChE Journal* **2002,** *48*, (10), 2366-2374.

19. Ngwenya, B. T.; Tourney, J.; Magennis, M.; Kapetas, L.; Olive, V., A surface complexation framework for predicting water purification through metal biosorption. *Desalination* **2009,** *248*, (1-3), 344-351.
20. Kapetas, L.; Ngwenya, B. T.; Macdonald, A. M.; Elphick, S. C., Kinetics of bacterial potentiometric titrations: The effect of equilibration time on buffering capacity of Pantoea agglomerans suspensions. *J. Colloid Interface Sci.* **2011,** *359*, (2), 481-486.
21. Tourney, J.; Ngwenya, B. T.; Mosselmans, J. W. F.; Tetley, L.; Cowie, G. L., The effect of extracellular polymers (EPS) on the proton adsorption characteristics of the thermophile Bacillus licheniformis S-86. *Chem. Geol.* **2008,** *247*, (1-2), 1-15.
22. Kohler, M.; Curtis, G. P.; Kent, D. B.; Davis, J. A., Experimental investigation and modeling of uranium (VI) transport under variable chemical conditions. *Water Resour. Res.* **1996,** *32*, (12), 3539-3551.
23. Yee, N.; Fein, J. B., Does metal adsorption onto bacterial surfaces inhibit or enhance aqueous metal transport? Column and batch reactor experiments on Cd-Bacillus subtilis-quartz systems. *Chem. Geol.* **2002,** *185*, (3-4), 303-319.
24. Lenhart, J. J.; Saiers, J. E., Transport of silica colloids through unsaturated porous media: experimental results and model comparisons. *Environ. Sci. Technol.* **2002,** *36*, (4), 769-777.
25. Xu, Y.; Axe, L., Synthesis and characterization of iron oxide-coated silica and its effect on metal adsorption. *J. Colloid Interface Sci.* **2005,** *282*, (1), 11-19.
26. Schwertmann, U., Iron oxides in the laboratory : preparation and characterization *2nd edition, Weinheim ; New York : Wiley-VCH,* **2000**.
27. Zachara, J. M.; Smith, S. C.; Kuzel, L. S., Adsorption and dissociation of Co-Edta complexes in Iron Oxide-containing subsurface sands. *Geochim. Cosmochim. Acta* **1995,** *59*, (23), 4825-4844.
28. Ngwenya, B. T.; Sutherland, I. W.; Kennedy, L., Comparison of the acid-base behaviour and metal adsorption characteristics of a gram-negative bacterium with other strains. *Appl. Geochem.* **2003,** *18*, (4), 527-538.
29. Alexander, M., *Introduction to soil microbiology.* New York: Wiley **1977**, p. 16-35.
30. Ghiorse, W. C.; Wilson, J. T., Microbial ecology of the terrestrial subsurface. *Adv Appl Micro 33:107-172.* **1988**.
31. Borrok, D.; Fein, J. B.; Tischler, M.; O'Loughlin, E.; Meyer, H.; Liss, M.; Kemner, K. M., The effect of acidic solutions and growth conditions on the adsorptive properties of bacterial surfaces. *Chem. Geol.* **2004,** *209*, (1-2), 107-119.
32. Gustafson, J. P., Visual-MINTEQ, version 2.30: *a windows version of MINTEQA2, version 4.0.* URL http://www.lwr.kth.se/english/OurSoftware/Vminteq. **2004**.
33. Herbelin, A. L.; Westall, J. C., *FITEQL 4.0: a computer program for determination of chemical equilibrium constants from experimental data.* Report 99–01 **1999,** Department of Chemistry Oregon State University, Corvallis.
34. Borrok, D. M.; Fein, J. B., The impact of ionic strength on the adsorption of protons, Pb, Cd, and Sr onto the surfaces of Gram negative bacteria: testing non-electrostatic, diffuse, and triple-layer models. *J. Colloid Interface Sci.* **2005,** *286*, (1), 110-126.
35. Bradford, S. A.; Yates, S. R.; Bettahar, M.; Simunek, J., Physical factors affecting the transport and fate of colloids in saturated porous media. *Water Resour. Res.* **2002,** *38*, (12), 1327.

36. Oliviera, I. B.; Demond, A. H.; Salehzadeh, A., Packing of sands for the production of homogeneous porous media. *Soil Sci Soc Am J* **1996,** *60*, (1), 49-53.
37. Simunek, J.; van Genuchten, M. T.; Sejna, M.; Toride, N.; Leij, F. J., *The STANMOD computer software for evaluating solute transport in porous media using analytical solutions of convection-dispersion equation.* U.S. Sanilinity Laboratory, Agricultural Research Service, U.S. Department of Agriculture, Riverside, California **1999**.
38. Yee, N.; Fowle, D. A.; Ferris, F. G., A Donnan potential model for metal sorption onto Bacillus subtilis. *Geochim. Cosmochim. Acta* **2004,** *68*, (18), 3657-3664.
39. Lai, C. H.; Lo, S. L.; Chiang, H. L., Adsorption/desorption properties of copper ions on the surface of iron-coated sand using BET and EDAX analyses. *Chemosphere* **2000,** *41*, (8), 1249-1255.
40. Daughney, C. J.; Fein, J. B.; Yee, N., A comparison of the thermodynamics of metal adsorption onto two common bacteria. *Chem. Geol.* **1998,** *144*, (3-4), 161-176.
41. Guiné, V.; Spadini, L.; Sarret, G.; Muris, M.; Delolme, C.; Gaudet, J. P.; Martins, J. M. F., Zinc sorption to three gram-negative bacteria: Combined titration, modeling, and EXAFS study. *Environ. Sci. Technol.* **2006,** *40*, (6), 1806-1813.
42. Ams, D.; Fein, J. B.; Dong, H.; Maurice, P. A., Experimental measurements of the adsorption of Bacillus subtilis and Pseudomonas mendocina onto Fe-oxyhydroxide-coated and uncoated quartz grains. *Geomicrobiol. J.* **2004,** *21*, 511-519.
43. Xu, S.; Liao, Q.; Saiers, J. E., Straining of nonspherical colloids in saturated porous media. *Environ. Sci. Technol.* **2008,** *42*, (3), 771-778.
44. Sakthivadivel, R., *Clogging of a granular porous medium by sediment.* Rep. No. HEL15-7, Hydraulic Engineering Lab., Univ. of California, Berkeley, Calif., 106 **1969**.
45. Bradford, S. A.; Bettahar, M.; Simunek, J.; van Genuchten, M. T., Straining and attachment of colloids in physically heterogeneous porous media. *VJZ* **2004,** *3*, (2), 384-394.
46. Tufenkji, N.; Miller, G. F.; Ryan, J. N.; Harvey, R. W.; Elimelech, M., Transport of cryptosporidium oocysts in porous media: Role of Straining and Physicochemical Filtration. *Environ. Sci. Technol.* **2004,** *38*, (22), 5932-5938.
47. Turner, B. F.; Fein, J. B., Appropriateness of equilibrium assumptions for determining metal distribution and transport in bacteria-bearing porous media. *Chem. Geol.* **2007,** *242*, (1-2), 40-50.
48. Grolimund, D.; Borkovec, M., Release of colloidal particles in natural porous media by monovalent and divalent cations. *J. Contam. Hydrol.* **2006,** *87*, (3-4), 155-175.
49. Roy, S. B.; Dzombak, D. A., Colloid release and transport processes in natural and model porous media. *Colloids Surf., A: Physicochemical and Engineering Aspects* **1996,** *107*, 245-262.
50. Cundy, A. B.; Hopkinson, L.; Whitby, R. L. D., Use of iron-based technologies in contaminated land and groundwater remediation: A review. *Sci. Total Environ.* **2008,** *400*, (1-3), 42-51.
51. Gupta, V. K.; Saini, V. K.; Jain, N., Adsorption of As(III) from aqueous solutions by iron oxide-coated sand. *J. Colloid Interface Sci.* **2005,** *288*, (1), 55-60.
52. Chen, M.; Li, X.-m.; Yang, Q.; Zeng, G.-m.; Zhang, Y.; Liao, D.-x.; Liu, J.-j.; Hu, J.-m.; Guo, L., Total concentrations and speciation of heavy metals in municipal sludge from Changsha, Zhuzhou and Xiangtan in middle-south region of China. *J. Hazard. Mater.* **2008,** *160*, (2-3), 324-329.

53. Pathak, A.; Dastidar, M. G.; Sreekrishnan, T. R., Bioleaching of heavy metals from sewage sludge: A review. *J. Environ. Manage.* **2009,** *90*, (8), 2343-2353.
54. Peng, G.; Tian, G.; Liu, J.; Bao, Q.; Zang, L., Removal of heavy metals from sewage sludge with a combination of bioleaching and electrokinetic remediation technology. *Desalination* **2011,** *271*, (1-3), 100-104.
55. Zhu, R.; Wu, M.; Yang, J., Mobilities and leachabilities of heavy metals in sludge with humus soil. *J. Environ. Sci.* **2011,** *23*, (2), 247-254.
56. Borrok, D.; Fein, J. B.; Kulpa, C. F., Proton and Cd adsorption onto natural bacterial consortia: testing universal adsorption behavior. *Geochim. Cosmochim. Acta* **2004,** *68*, (15), 3231-3238.
57. Borrok, D.; Turner, B. F.; Fein, J. B., A universal surface complexation framework for modeling proton binding onto bacterial surfaces in geologic settings. *Am. J. Sci.* **2005,** *305*, (6-8), 826-853.
58. Johnson, K. J.; Szymanowski, J. E. S.; Borrok, D.; Huynh, T. Q.; Fein, J. B., Proton and metal adsorption onto bacterial consortia: Stability constants for metal-bacterial surface complexes. *Chem. Geol.* **2007,** *239*, (1-2), 13-26.
59. Daughney, C. J.; Fowle, D. A.; Fortin, D., The effect of growth phase on proton and metal adsorption by Bacillus subtilis. *Geochim. Cosmochim. Acta* **2001,** *65*, (7), 1025-1035.
60. Heinrich, H. T. M.; Bremer, P. J.; McQuillan, A. J.; Daughney, C. J., Modelling of the acid-base properties of two thermophilic bacteria at different growth times. *Geochim. Cosmochim. Acta* **2008,** *72*, (17), 4185-4200.
61. Takahashi, Y.; Châtellier, X.; Hattori, K. H.; Kato, K.; Fortin, D., Adsorption of rare earth elements onto bacterial cell walls and its implication for REE sorption onto natural microbial mats. *Chem. Geol.* **2005,** *219*, (1-4), 53-67.
62. Tourney, J.; Ngwenya, B. T.; Fred Mosselmans, J. W.; Magennis, M., Physical and chemical effects of extracellular polymers (EPS) on Zn adsorption to Bacillus licheniformis S-86. *J. Colloid Interface Sci.* **2009,** *337*, (2), 381-389.
63. Kim, S.-B.; Corapcioglu, M. Y., Contaminant transport in riverbank filtration in the presence of dissolved organic matter and bacteria: a kinetic approach. *J. Hydrol.* **2002,** *266*, (3-4), 269-283.
64. Abudalo, R. A.; Ryan, J. N.; Harvey, R. W.; Metge, D. W.; Landkamer, L., Influence of organic matter on the transport of Cryptosporidium parvum oocysts in a ferric oxyhydroxide-coated quartz sand saturated porous medium. *Water Res.* **2010,** *44*, (4), 1104-1113.
65. Hall, J. A.; Mailloux, B. J.; Onstott, T. C.; Scheibe, T. D.; Fuller, M. E.; Dong, H.; DeFlaun, M. F., Physical versus chemical effects on bacterial and bromide transport as determined from on site sediment column pulse experiments. *J. Contam. Hydrol.* **2005,** *76*, (3-4), 295-314.
66. Fang, L.; Cai, P.; Li, P.; Wu, H.; Liang, W.; Rong, X.; Chen, W.; Huang, Q., Microcalorimetric and potentiometric titration studies on the adsorption of copper by P. putida and B. thuringiensis and their composites with minerals. *J. Hazard. Mater.* **2010,** *181*, (1-3), 1031-1038.
67. Hand, V. L.; Lloyd, J. R.; Vaughan, D. J.; Wilkins, M. J.; Boult, S., Experimental Studies of the Influence of Grain Size, Oxygen Availability and Organic Carbon Availability on Bioclogging in Porous Media. *Environ. Sci. Technol.* **2008,** *42*, (5), 1485-1491.
68. Liu, Y.; Yang, C. H.; Li, J., Influence of extracellular polymeric substances on Pseudomonas aeruginosa transport and deposition profiles in porous media. *Environ. Sci. Technol.* **2007,** *41*, (1), 198-205.

69. Long, G.; Zhu, P.; Shen, Y.; Tong, M., Influence of Extracellular Polymeric Substances (EPS) on deposition kinetics of bacteria. *Environ. Sci. Technol.* **2009,** *43*, (7), 2308-2314.

Table 1. Retardation factors are presented for the breakthrough curves of Zn in the control experiments (absence of cells), total Zn and free aqueous Zn of the co-transport experiments presented in Figures 1 and 2. Retardation factors were calculated using an equilibrium model (CFITIM, Stanmod [37]) for simplicity. Associated error represents the standard error of the regression coefficient (±1s.e.). The number of PVs flowed to reach steady state, the relative concentration C/C_o of cell breakthrough and the percentage of mobile cell-bound zinc at steady state conditions are reported based on the BTCs of Figures 1 and 2. Errors associated with the percentage values represent 1σ calculated from the data steady state has been reached.

Figure 1. Zinc and cell BTCs from co-transport experiments carried out at (A) pH 7 and *I* 0.01 M using clean sand columns, (B) pH 5.3 and *I* 0.01 M using IOCS columns and (C) pH 7 and *I* 0.01 M using IOCS columns. Influent Zn and cell concentrations were 1.53×10^{-4} M and 0.5 g L^{-1} respectively. Free zinc represents aqueous zinc while total zinc represents the sum of free and mobile cell-bound zinc. Cell, free and total zinc BTC results are shown with triangle, square and circle symbols respectively. The BTC of the bromide conservative tracer is presented with "+" symbols and the BTC of 1.53×10^{-4} M Zn in the absence of cells (control) is provided for comparison with "x" symbols.

Figure 2. Breakthrough curves of zinc/cell co-transport. Experiment was carried out at pH 7 and *I* 0.01 M using an IOCS column and cells and zinc were pre-equilibrated in the influent. Influent total Zn and cell concentrations were 1.53×10^{-4} M and 0.5 g L^{-1} respectively. Free zinc represents aqueous zinc while total zinc represents the sum of free and mobile cell-bound zinc. Cell, free and total zinc BTC results are shown with black triangle, square and circle symbols respectively. The BTC of the bromide conservative tracer is presented with "**+**" symbols and the BTC of 1.53×10^{-4} M Zn in the absence of cells (control) is provided for comparison with "**x**" symbols.

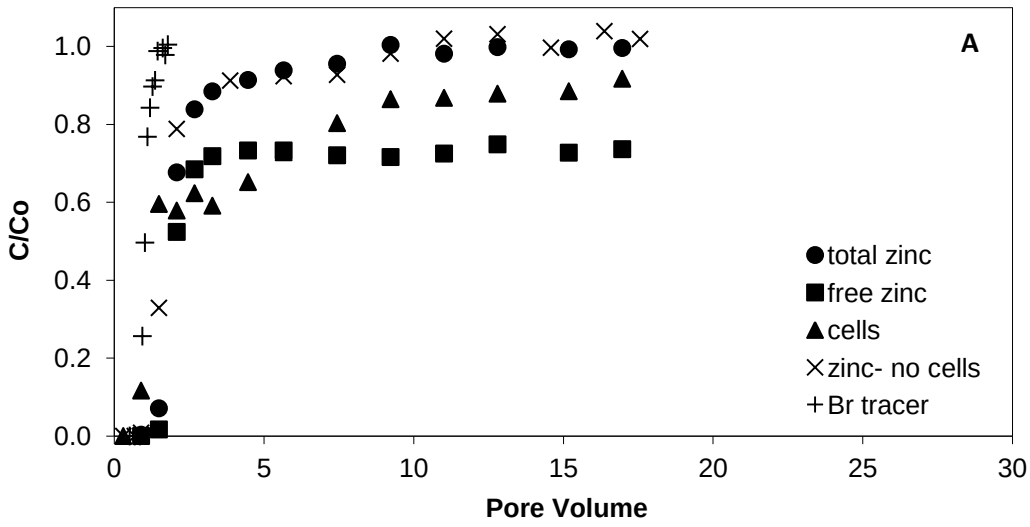
A
C/Co
Pore Volume
0.0
0.2
0.4
0.6
0.8
1.0
0
5
10
15
20
25
30
total zinc
free zinc
cells
zinc- no cells
Br tracer

Figure 1A.

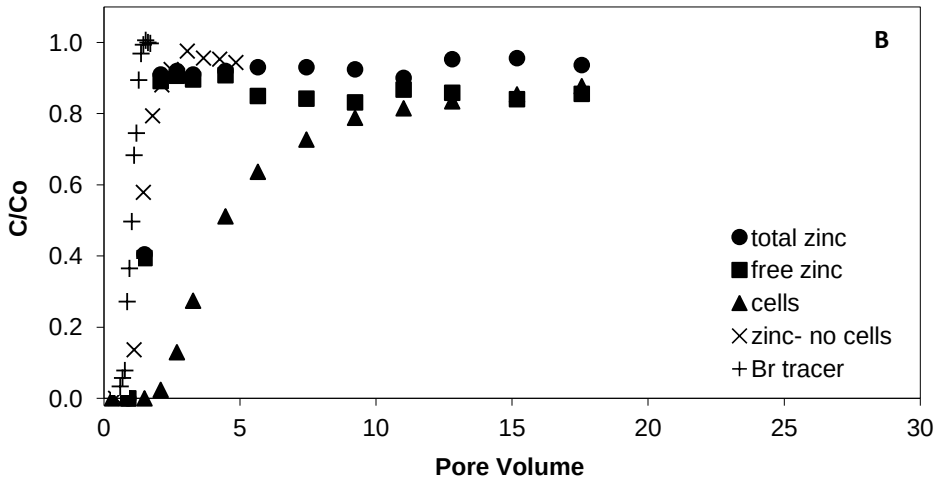
B
C/Co
Pore Volume
total zinc
free zinc
cells
zinc- no cells
Br tracer
0.0
0.2
0.4
0.6
0.8
1.0
0
5
10
15
20
25
30

Figure 1B.

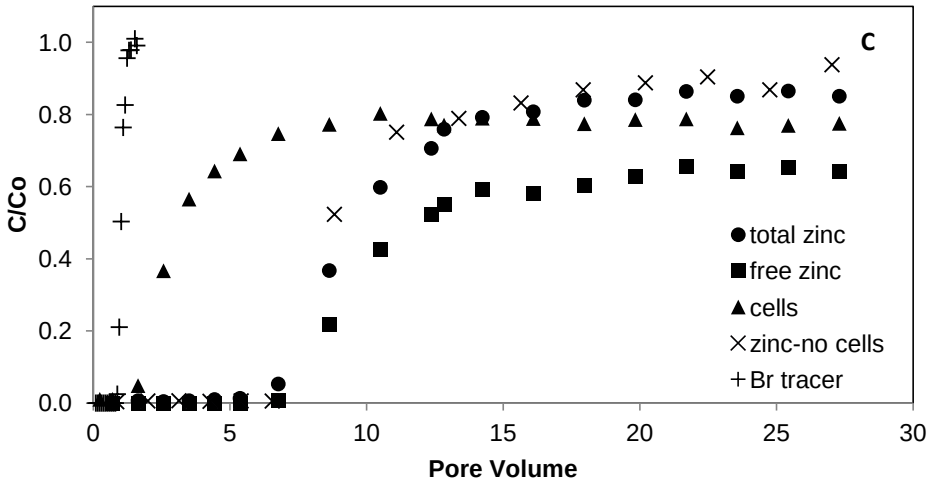
C
C/Co
1.0
0.8
0.6
0.4
0.2
0.0
0
5
10
15
20
25
30
Pore Volume
total zinc
free zinc
cells
zinc-no cells
Br tracer

Figure 1C.

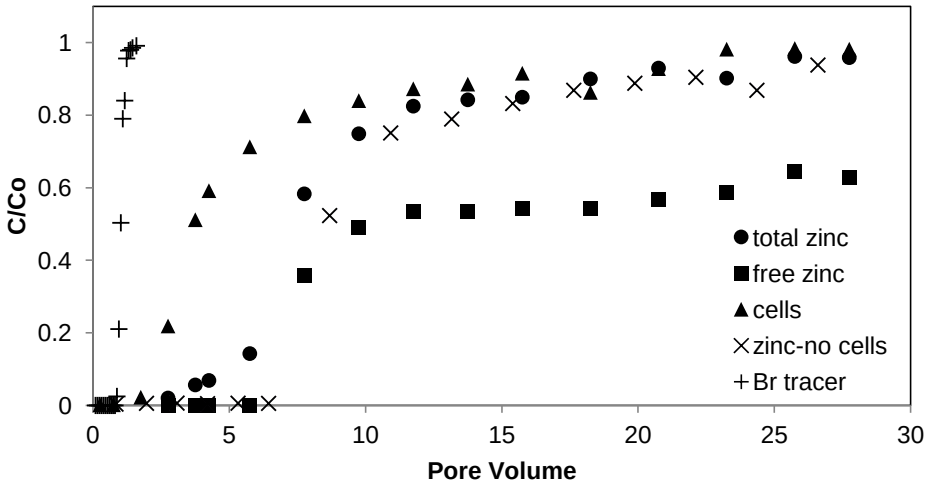
C/Co
Pore Volume
0
0.2
0.4
0.6
0.8
1
0
5
10
15
20
25
30
total zinc
free zinc
cells
zinc-no cells
Br tracer

Figure 2.

Experimental conditions	Ret. Factor Zn-no cells	Ret. Factor Total Zn	Ret. Factor Free Zn	PVs to steady state	Steady state C/Co cell BT	Cell bound Zn at steady state (%)	PVs to 50% cell BT
Clean Sand; pH 7 (Fig 1A)	1.58±0.04	1.97±0.04	1.95±0.02	9	0.85	26±1	1.35
IOCS; pH 5.3 (Fig. 1B)	1.42±0.04	1.54±0.03	1.50±0.01	9	0.8	9±3	4.35
IOCS; pH 7 (Fig. 1C)	8.88±0.31	10.15±0.68	9.71±0.22	16	0.75	26±2	3.3
IOCS; pH 7, Zn-cell pre-association (Fig. 2)	8.88±0.31	7.60±0.25	7.63±0.20	16	0.9	36±3	3.7

Table 1

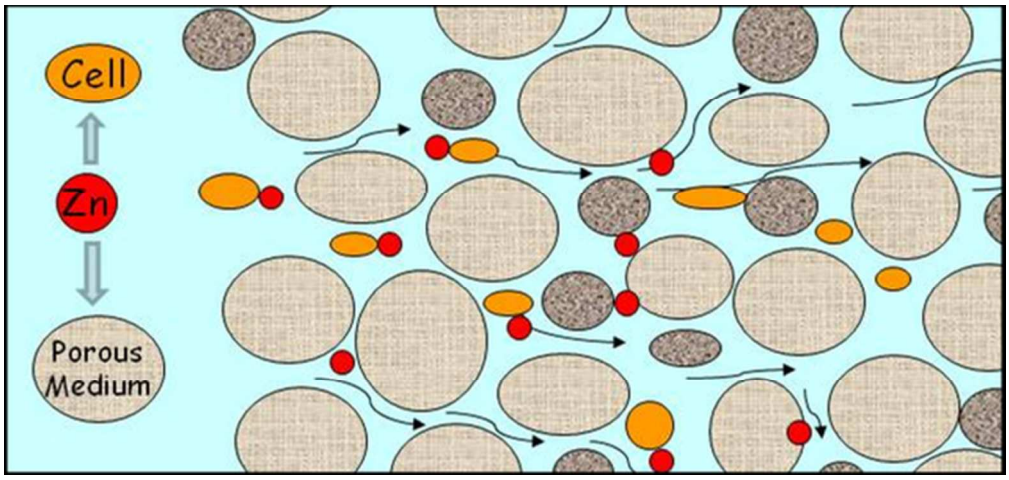

84x39mm (300 x 300 DPI)